Title

Nucleation of soot: experimental assessment of the role of polycyclic aromatic hydrocarbon (PAH) dimers

Journal

Zeitschrift für Physikalische Chemie, 234(7-9)

ISSN

0942-9352

Authors

Adamson, Brian A
Skeen, Scott A
Ahmed, Musahid
et al.

Publication Date

2020-07-01

DOI

10.1515/zpch-2020-1638

Peer reviewed

Nucleation of Soot: Experimental Assessment of the Role of Polycyclic Aromatic Hydrocarbon (PAH) Dimers

B. A. Adamson,[a)] S. A. Skeen,[a)] M. Ahmed,[b)] N. Hansen[a)]*

[a)] Combustion Research Facility, Sandia National Laboratories, Livermore, CA 94551, USA

[b)] Chemical Sciences Division, Lawrence Berkeley National Laboratory, Berkeley, CA 94720, USA

submitted to

Zeitschrift für Physikalische Chemie
Friedrich Temps Festschrift

21 Pages

8 Figures

[*] Corresponding author (NH): nhansen@sandia.gov, phone: +1 925 294 6272

Abstract:

The irreversible dimerization of polycyclic aromatic hydrocarbons (PAHs) – typically pyrene ($C_{16}H_{10}$) dimerization - is widely used in combustion chemistry models to describe the soot particle inception step. This paper concerns itself with the detection and identification of dimers of flame-synthesized PAH radicals and closed-shell molecules and an experimental assessment of the role of these PAH dimers for the nucleation of soot. To this end, flame-generated species were extracted from an inverse co-flow flame of ethylene at atmospheric pressure and immediately diluted with excess nitrogen before the mixture was analyzed using flame-sampling tandem mass spectrometry with collision-induced fragmentation. Signal at *m/z* = 404.157 ($C_{32}H_{20}$) and *m/z* = 452.157 ($C_{36}H_{20}$) were detected and identified as dimers of closed-shell $C_{16}H_{10}$ and $C_{18}H_{10}$ monomers, respectively. A complex between a $C_{13}H_9$ radical and a $C_{24}H_{12}$ closed-shell PAH was observed at *m/z* = 465.164 ($C_{37}H_{21}$). However, a rigorous analysis of the flame-sampled mass spectra as a function of the dilution ratio, defined as the ratio of the flow rates of the diluent nitrogen to the sampled gases, indicates that the observed dimers are not flame-born, but are produced in the sampling line. In agreement with theoretical considerations, this paper provides experimental evidence that pyrene dimers cannot be a key intermediate in particle inception at elevated flame temperatures.

Introduction:

Soot formation remains an intriguing phenomenon that covers a broad range of physical-chemistry aspects. In a simplified scheme, chemical reactions in the gas phase lead to polycyclic aromatic hydrocarbons (PAHs) and, following the transition from gas-phase species to solid particles, the so-called particle inception, multi-phase surface growth reactions and physical coagulation become important.[1-4] Significant progress has been made towards understanding the gas-phase chemistry of PAH formation in the high-temperature environment of flames.[5-8] It is well understood that the chemistry is governed by radical-radical and radical-molecule reactions,[9-15] although the details about reaction rates, product branching ratios, and their implementation in chemically detailed mechanisms are still being worked out.[16-23]

A similar level of understanding has not been achieved for the chemistry and physics of the particle inception step and several hypotheses are awaiting experimental validation and are still discussed controversially.[1-4] The most widely accepted hypothesis is based on the irreversible dimerization of polycyclic aromatic hydrocarbons, which has been implemented in many combustion chemistry models using pyrene as the dimerizing intermediate. This proposed scenario, in which stacked pyrene (or more generally, PAH) dimers are irreversibly formed and bound by van der Waals forces, originates from the seminal work of Frenklach and co-workers.[3, 10, 24]

Despite the lack of strong experimental evidence supporting this hypothesized nucleation step, the inclusion of the dimerization reaction helps to explain the nuclei formation at low temperatures and the observed mean particle size of soot particles. However, experimental and theoretical evidence is emerging now that challenge the general results of the PAH dimerization model.[25-28] For example, theoretically determined equilibrium constants and lifetimes of the PAH dimers at these high flame temperatures indicate that pyrene dimerization is unlikely to play a role in the particle inspection step. PAHs larger than 600 to 800 amu would be needed to form dimers that can sustain flame temperatures.[29-

[30] However, given the fact that the concentrations of large PAHs in flames are kinetically limited, the low concentrations of these intermediates cast doubt on a dominant role in soot nucleation and consequently this theory of PAH dimerization is widely disputed.[27]

To overcome the simplifying assumption of irreversibility in the hypothesized dimerization model, Miller and Eaves *et al.* introduced the concept of reversibility.[30-32] They added a chemical bond formation term that describes the formation of chemical bonds between PAHs and thus the scientific discussion currently shifts towards aliphatically bridged PAHs.[28, 33-34] These hypothesized compounds have only recently been identified in flame-sampling tandem mass spectrometry experiments.[35] In the same work, aliphatically substituted PAHs were identified, which might be of significance for particle inception as Violi and coworkers have shown that their dimers are more likely to survive elevated flame temperatures.[25, 36]

While the importance of these recently detected aliphatically substituted and bridged PAHs for particle inception remains to be determined in future modeling work, many mechanisms still rely on irreversible dimerization of PAHs as small as pyrene as the nucleation step. In this work, we use flame-sampling tandem mass spectrometry to critically assess the role of PAH dimers in the process of soot nucleation. Because of the need to sample out of the high-temperature environment of a flame, the immediate dilution of the sampled species is discussed as an important factor to avoid risk of misinterpretation of the observed mass spectra. We show how tandem mass spectrometry can be used to detect and identify PAH dimers, and then provide experimental evidence supporting earlier theoretical work[26-27, 37-40] that pyrene dimers do not exist in flames.

Experimental Methods:

The results on the PAH dimers discussed here were obtained using the flame-sampling tandem mass spectrometer implemented by Adamson *et al.* for the detection of alkyl substituted and aliphatically bridged PAHs.[35] The details of the experimental set-up were described in that earlier work and only a short

description is given here: The mass spectrometer consists of an atmospheric pressure photoionization (APPI) source, a quadrupole mass filter, a collision cell filled with Ar for the collision induced dissociation (CID) process, and a reflectron time-of-flight spectrometer to separate the ions. In the APPI source the flame-sampled species are ionized using 10.0 eV photons from a continuous vacuum-ultraviolet (VUV) Kr discharge lamp. This energy is sufficient to ionize the aromatic species and their dimers as discussed in the next Section. The resulting ions are subsequently sampled into the high vacuum of the mass spectrometer. The quadrupole mass filter can be operated in either an ion guide mode when an overview spectrum was to be collected, or in a mass-selective mode (Δm ~ 1), when MS-MS spectra were to be obtained. To the first mode, we refer here as "TOF" mode, whereas the second mode of operation is referred to as "MS-MS" mode. After the quadrupole mass filter, the ions of the respective flame-sampled components are accelerated into the argon-filled CID cell, where they can undergo fragmentation into a neutral and an ion fragment. The velocity of the ions, *i.e.* the collision energy, can be scanned automatically to allow for an assessment of the respective strength of the breaking bond. The fragment ion is then extracted into a high-resolution reflectron time-of-flight mass spectrometer ($m/\Delta m$ ~ 8000) and these fragment mass spectra can be used to extract structural information on the sampled flame components. Given the discriminator settings on the multi-channel scaler, almost background-free mass spectra can be recorded leading to signal-to-noise ratios that are sufficient to clearly revealing the PAH dimers and their monomers as described below.

For the experiments described here, we used the same inverse co-flow diffusion flame of ethylene (C_2H_4) as described in the earlier work.[35] The burner geometry and the gas flows were as follows: The stainless-steel burner consists of three concentric tubes with inner diameters of 14, 20, and 50 mm, respectively. The respective gas flows were: 240 sccm O_2 diluted in 960 sccm N_2 through the inner tube, 310 sccm C_2H_4 diluted with 1000 sccm of N_2 through the second concentric ring, and 20 slm of a sheath N_2 flow through the outer ring. The gases were purchased from Matheson with a purity of more than

99.99%. The flame was kept at atmospheric pressure, with the entire burner assembly housed in a fixed chimney on a motor-controlled x-y translational stage. With an accuracy of ±0.05 mm, this assembly allowed for sampling of flame species at all positions in the flame through a 0.1 mm pin hole in a stainless-steel tube and, before flowing into the APPI source, they were diluted immediately with N_2 at various flow rates, spanning a dilution ratio of 200 to 1500. The sampling position is ~40 cm away from the ionization region in the APPI and the transfer tube was not heated.

While in Ref. [35] we described that the observed flame-sampled MS-MS spectra are consistent with alkyl-substituted and aliphatically bridged PAH structures, in this paper we describe how flame-sampling tandem mass spectrometry allows for gaining insights into soot nucleation and particle inception.

Results and Discussion:

The present paper has two main objectives, which are (a) to describe the detection and identification of dimers of flame-generated PAH molecules and radicals and (b) to assess the role of PAH dimers for soot nucleation. In the first part of this project, we used flame-synthesized PAH molecules to develop a detection method for PAH dimers based on tandem mass spectrometry. Based on this knowledge, in the second part, we explore the role of pyrene dimerization in the formation of soot.

(a) Detection and Identification of PAH Dimers:

Using the tandem mass spectrometer, we were able to detect and identify PAH dimers after sampling from the laboratory flame. Because of the wide-spread use of pyrene dimerization in many combustion chemistry soot models, we start our discussion with the identification of the observed mass spectral signal at m/z = 404.157 ($C_{32}H_{20}$).

For the experiments discussed here, we sampled from the ethylene co-flow diffusion flame with low dilution and operated the mass spectrometer in the mass-selective MS-MS mode, selecting m/z = 404 using the quadrupole mass filter. A three-dimensional plot of the flame-sampled MS-MS spectra of *m/z* = 404.157 ($C_{32}H_{20}$) is shown in Fig. 1 (left). In this plot, the ion intensity is shown as function of the mass-to-charge ratio (x-axis) and the collision energy (on the y-axis). The plot clearly reveals signal at *m/z* = 404.157 is stable at low collision energies but then it fragments at relatively low collision energy into *m/z* = 202.078 ($C_{16}H_{10}$) fragments, supporting the identification of the detected $C_{32}H_{20}$ component as $C_{16}H_{10}$ dimer.

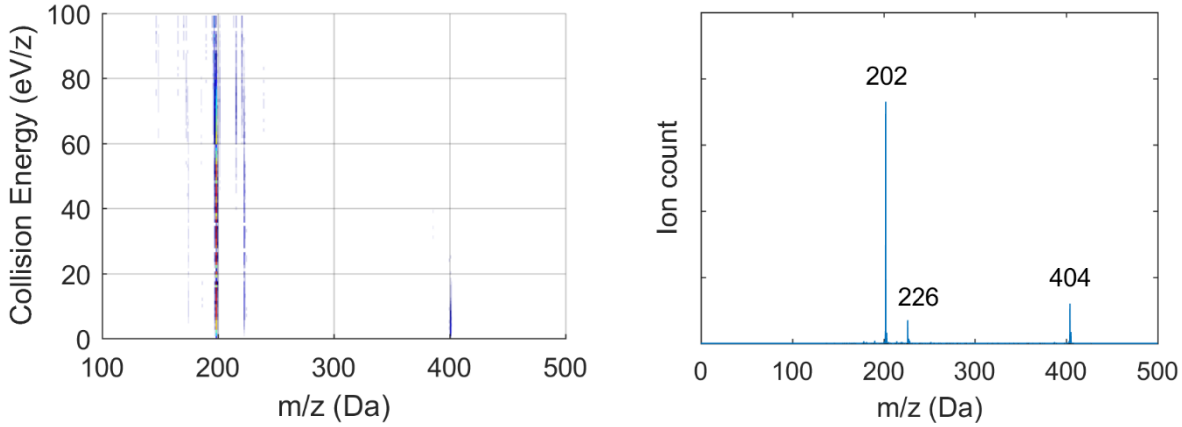

Figure 1: Left: Flame-sampled MS-MS of *m/z* = 404.157 ($C_{32}H_{20}$). Fragmentation into *m/z* = 202.078 ($C_{16}H_{10}$) at low collision energies is visible. Also, the MS-MS reveals that $C_{32}H_{20}$ consists of $C_{14}H_{10}$ + $C_{18}H_{10}$ dimers. Right: High-resolution integrated mass spectra at low collision energies from 0-10 eV/z.

Especially the very low collision energy needed to break the *m/z* = 404.157 complex, indicates that $C_{32}H_{20}$ is a weakly bound complex. As seen in Fig. 1 (left), the signal of the parent ion at *m/z* = 404.157 disappears below 20 eV/z. It is shown in Ref. [35] that collision energies of 20 eV/z are typically required to break C-C single bonds on the ion potential energy surface and that even higher energies of at least ~40 eV/z are needed to fragment the aromatic ring. Because in these experiments the PAH-PAH$^+$ dimer is fragmented, it is important to note that the observed appearance energies of the fragment ions cannot be easily correlated to the binding energies of the neutral PAH-PAH dimer.

Furthermore, the MS-MS also revealed that the *m/z* = 404.157 complex contains PAH dimers of monomers at *m/z* = 226.078 ($C_{18}H_{10}$) – with a *m/z* = 178.078 ($C_{14}H_{10}$) counter fragment. Because the charge

of the ion is most likely to stay on the larger fragment, in this case the *m/z* = 226.078 fragment, the different signal intensities of the $C_{14}H_{10}$ and $C_{18}H_{10}$ fragments are important, as it indicates that indeed the dimers are ionized according to Eq. 1 and not that ions are forming dimers as shown in Eq. 2:

$$PAH + PAH \dashrightarrow Dimer \dashrightarrow Dimer^{+} \quad \text{(Eq. 1)}$$

$$PAH^{+} + PAH \dashrightarrow Dimer^{+} \quad \text{(Eq. 2)}$$

Further evidence for this interpretation is shown below when the dilution experiments are discussed.

Fig. 1 (right) shows the high-resolution tandem mass spectra integrated over low collision energies from 0-10 eV/z. Clearly visible are the parent ion of *m/z* = 404.157 and the collision-induced fragment ions at *m/z* = 202.078 ($C_{16}H_{10}$) and 226.078 ($C_{18}H_{10}$).

Additional conformation for the *m/z* = 404.157 signal originating from PAH dimers can be found in the two-dimensional intensity profiles of *m/z* = 178.0178, 202.0178, and 226.0178 as function of the collision energy as shown in Fig. 2. This figure clearly reveals that (a) the constituents are bound relatively weakly as the respective fragment ions are clearly formed at low collision energies and that (b) the respective signals are highly correlated to each other. The observed oscillations are caused by experimental instabilities, but they turn out to be really useful to prove the point that the signal is heavily

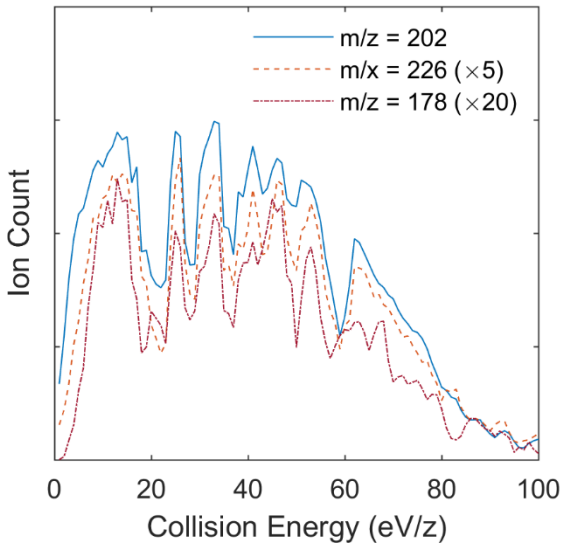

Figure 2: Ion intensities of *m/z* = 202, 226, and 178 as a function of the collision energy.

correlated. Furthermore, Adamson *et al.*[35] have shown in their previous work that *m/z* = 202.078 ($C_{16}H_{10}$) ions tend to dissociate at collision energies beyond ~40 eV/z, which is consistent with the results shown in Fig. 2, thus explaining the decrease in ion signal with higher collision energies. In summary, the provided experimental results are consistent with the signal being attributed to weakly bound complexes.

The identity of the *m/z* = 202.078 signal cannot be revealed given the current knowledge of the collision-induced MS-MS spectra of $C_{16}H_{10}$ isomers, but pyrene and fluoranthene are likely components as they have been identified in other experiments using gas-chromatography and laser induced fluorscence.[41-43] Given the observed large collision energies needed for fragmentation, the experimental results indicate that the respective molecules are peri-condensed polycyclic aromatic hydrocarbons. To facilitate the discussion, Fig. 3(a) depicts structures for the plausible $C_{14}H_{10}$ isomers anthracene and phenanthrene, the pyrene and fluoranthene ($C_{16}H_{10}$), and cyclopenta[cd]pyrene ($C_{18}H_{10}$). The sandwich-

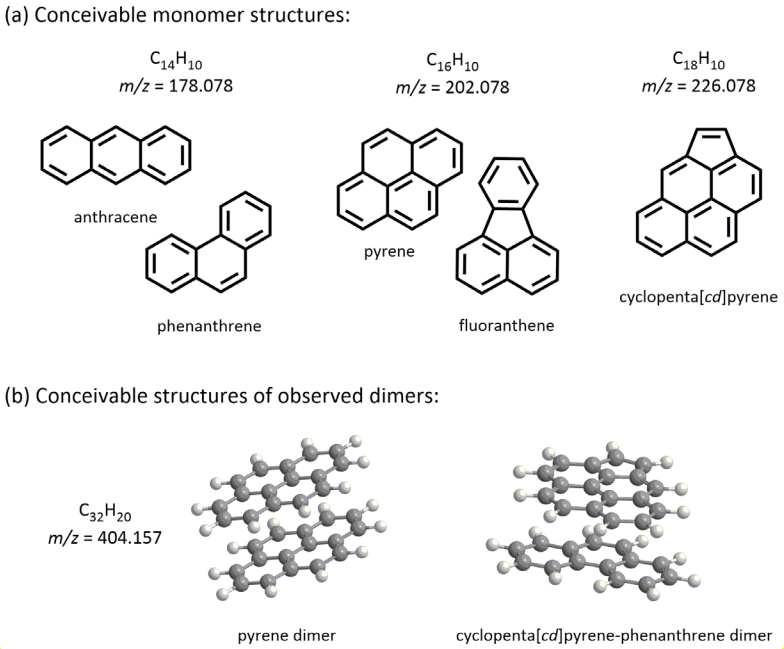

Fig. 3: (a) Conceivable monomer structures of $C_{14}H_{10}$ (*m/z* = 178.078) $C_{16}H_{10}$ (*m/z* = 202.078) and $C_{18}H_{10}$ (*m/z* = 226.078) intermediates. More $C_{18}H_{10}$ isomers are shown in Fig. 5. (b) conceivable structures of observed dimers at $C_{32}H_{20}$ (*m/z* = 404.157)

like structures of the pyrene dimer and the cyclopenta[cd]pyrene-phenanthrene dimer are shown in Fig. 3b.

A second example of PAH dimers that were detected by the flame-sampling tandem mass spectrometer is shown in Fig. 4 for *m/z* = 452.157 ($C_{36}H_{20}$). As for the previous example, the mass spectra were recorded with a small dilution ratio and in the MS-MS mode, specifically filtering out *m/z* = 452 ions. The left diagram in Fig. 4 shows the signal intensities as a function of mass-to-charge ratio (x-axis) and the collision energy (y-axis). The plot on the right shows the high-resolution integrated mass spectra at low collision energies from 0-10 eV/z. The collision-induced fragmentation patterns clearly reveal that the $C_{36}H_{20}$ species at low collision energies mainly fragment into *m/z* = 226.078 ($C_{18}H_{10}$) isomers, thus supporting the interpretation of *m/z* = 452.157 being due to PAH dimers. A complete interpretation of the MS-MS spectra shown in Fig. 4 is currently not possible and outside the scope of this work. However, we noticed that the additional fragments at higher collision energies appear at lower masses than *m/z* = 226.078, thus indicating that these signals are likely due to collision induced fragmentation of the monomeric structure.

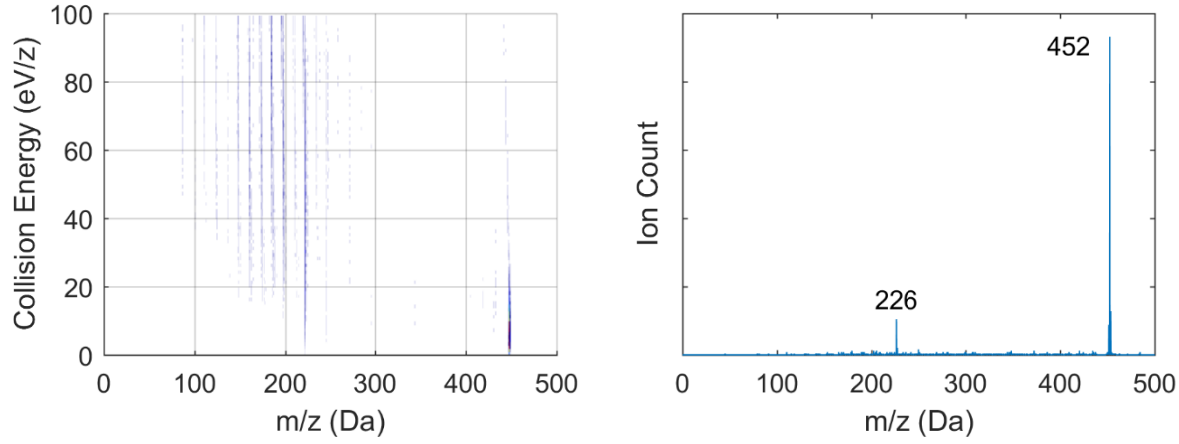

Figure 4: Left: Flame-sampled MS-MS of *m/z* = 452.157 ($C_{36}H_{20}$). Among others, the dissociation into *m/z* = 226.078 ($C_{18}H_{10}$) is apparent. Right: High-resolution integrated mass spectra at low collision energies from 0-10 eV/z.

Without a more fundamental understanding of the dissociation dynamics of the respective fragment ions at *m/z* = 226.078, a complete analysis seems rather impossible. Nevertheless, we noticed that the observed peaks at large collision energies are identical to the observed core-PAH structures that were reported by Adamson et al.[35] However, the complexity of the MS-MS spectra also indicates that the $C_{18}H_{10}$ signal is likely not due to only the stabilomer grid as proposed by Stein and Fahr.[44] The presence of non-stabilomer molecules has been widely accepted now in PAH growth chemistry.[45] Conceivable monomeric structures are shown in Fig. 5, to increase awareness of the complexity of structures that can be involved in PAH formation chemistry. This figure contains structures that are not included in Fig. 3, but by no means should be considered complete.

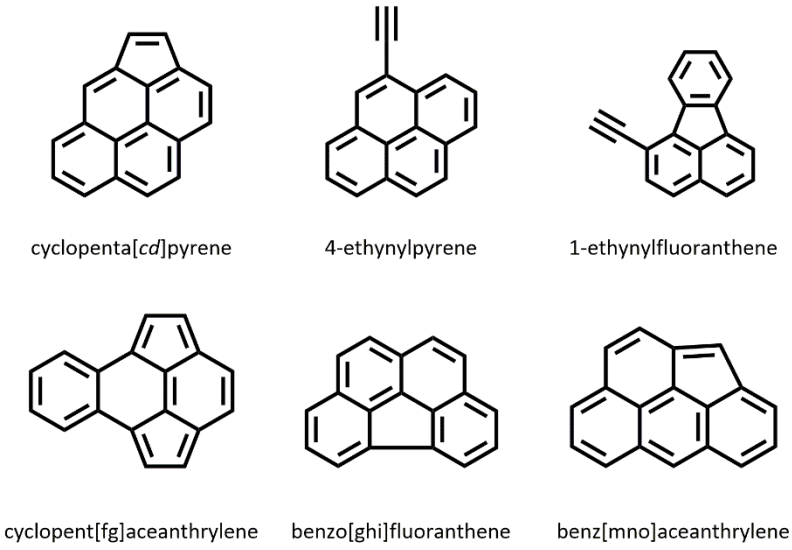

Figure 5: Conceivable monomer structures of $C_{18}H_{10}$ (*m/z* = 226.078) intermediates. This figures shows isomeric structures of the $C_{18}H_{10}$ isomer, cyclopenta[cd]pyrene , shown in Fig. 3.

In addition to the described detection of dimers of closed-shell PAH molecules, under the same experimental configuration, we detected PAH radical-molecule dimers. As evidence we show in Fig. 6 the integrated flame-sampled MS-MS fragmentation mass spectrum of *m/z* = 465.164 ($C_{37}H_{21}$). The small peak at *m/z* = 165.070 ($C_{13}H_9$) is likely to be a monomeric PAH radical resulting from a loss of a $C_{14}H_{12}$ counterpart. Typically, $C_{14}H_{12}$ is considered to be coronene, a very stable and peri-condensed PAH

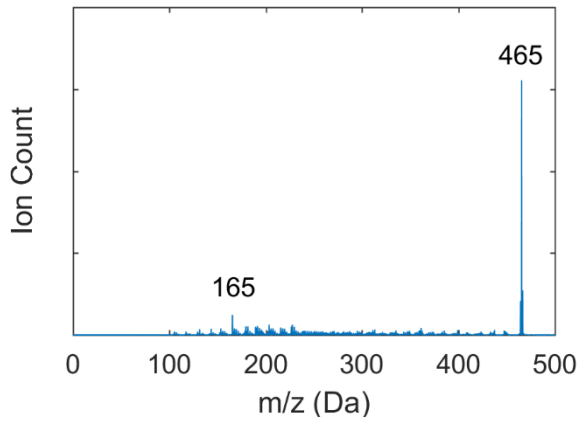

Figure 6: Integrated flame-sampled fragmentation mass spectrum of *m/z* = 465.164 ($C_{37}H_{21}$) in the collision energy range from 0-10 eV. The fragment at *m/z* = 165.070 ($C_{13}H_9$) corresponds to a loss of a neutral $C_{24}H_{12}$ molecule.

molecule at *m/z* = 300.094. Interestingly, the mass spectra indicate that for the dissociative collision, the charge stays with the ion and not with the larger fragment, as has been seen for the closed-shell dimers. The $C_{13}H_9$ radical species has been observed before in flame-sampling mass spectrometry experiments.[46] Its prominent appearance in flame environments is probably a result of its resonance-stabilization. A few possible isomeric forms are shown in Fig. 7 together with two conceivable *m/z* = 300.094 ($C_{24}H_{12}$) isomers.

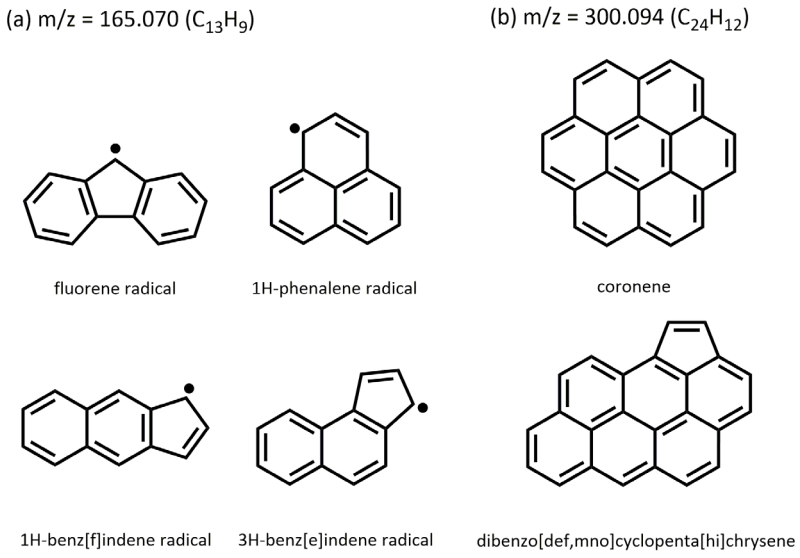

Figure 7: Conceivable monomer structures of (a) $C_{13}H_9$ and (b) $C_{24}H_{12}$ intermediates.

These three examples discussed here clearly demonstrate our capabilities to detect PAH-PAH dimers and PAH radical-PAH dimers. Next, we will apply this knowledge for assessing the role of these dimers in soot nucleation processes.

(b) Assessment of the Role of PAH Dimers for Soot Formation:

In the second part of this paper, the knowledge about how to detect and identify PAH dimers using tandem-mass spectrometry is used to assess the role of such PAH dimers for soot nucleation. For a meaningful discussion about this important process, a more detailed description of the probe-sampling experiments seems warranted.

While very detailed chemical insights can be gained from flame-sampling experiments, the interpretation of the results is certainly not trivial.[47] The sampling probe perturbs the flame structure, that is, most noticeably, the flow field, flame temperature and chemistry are impacted.[48-50] In the experiments presented here, we used a stainless-steel quarter inch tube with a small pinhole of 100 μm diameter facing the center of the burner outlet. As described previously in the literature for complementary soot sampling experiments,[51-54] such experimental set-up can create additional potential problems that range from PAH losses in the sample probe through PAH-PAH dimerization and to diffusive wall losses along the sampling line. To minimize these effects that significantly contribute to the inaccuracies of the experiment, the sampled flames gases are typically diluted as quickly as possible. A dilution ratio (ratio of the standard volumetric flow rate of nitrogen to the sampled gases) of up to 1000 is typically used to quench dimerization and other chemical reactions along the sampling line. In the experiments described here, the dilution ratio was changed by adjusting the flow rate of the N_2 diluent while keeping everything else unchanged.

The results of such dilution experiments are shown in Fig. 8. Here, ion signals for $C_{16}H_{10}$ (monomer), $C_{32}H_{20}$ ($C_{16}H_{10}$ dimers), and $C_{36}H_{20}$ ($C_{18}H_{10}$ dimers) were recorded in the TOF mode and are

shown as a function of time. The time responds to different dilution ratios, as for these experiments the N_2 diluent gas flow was constantly changed over time from large flow rates (left, t = 0 s) to smaller flow rates (right, t = 200s). That is, the dilution ratio is decreasing from left (~1500) to right (~200). At early times, *i.e.* high N_2 flow rates and high dilution ratios, no signal is observed, which is caused by the N_2 flow rates and the pumping speed of the APPI source leading to a pressure increase that actually pushes gas out through the sampling pinhole rather than flame species being sucked in. Once N_2 flow rates and pumping speed are balanced, gases are sampled from the flame and the respective ion signal for the flame-sampled $C_{16}H_{10}$ species relatively quickly reaches a maximum. The observed decrease in ion signal intensity with decreasing dilution ratios indicates losses on walls, coagulation or any other reaction. The extent of this loss seems to be linearly proportional to the decrease of the dilution ratio.

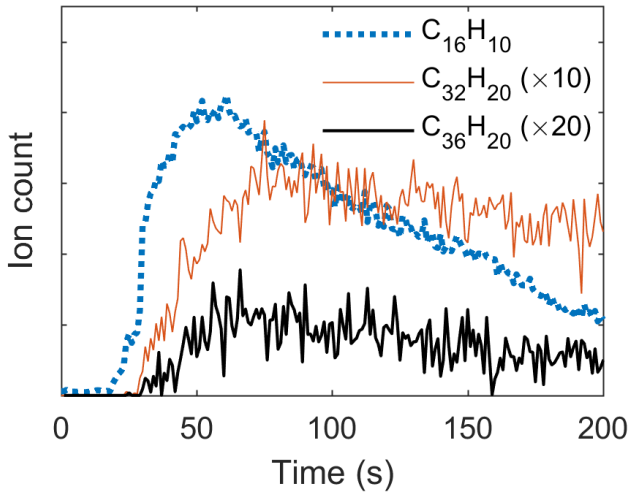

Figure 8: Dilution curves – ion signal as a function of time, *i.e.* dilution ratio

For any other flame-sampled species one would expect a similar trend in ion signal intensity. However, the profiles for the $C_{32}H_{20}$ and $C_{36}H_{20}$ dimers are significantly different than the one for the $C_{16}H_{10}$ monomer. As seen in Fig. 8, after a slower rise in signal intensity at shorter times (high dilution), the signal appears to be almost constant for a longer period of time. The observed different trends for monomers

and dimers indicate that the dimers are not flame-sampled species. The almost constant signal intensity profiles for the dimers are explained by partial compensation of the expected loss of the dimers (due to the same reasons as for the monomer) via the formation of additional dimers.

These results clearly indicate that the observed PAH dimers are not flame-generated but are an artifact of the sampling process. Knowing what to look for, the search for flame-sampled dimers was unsuccessful, in agreement with previous theoretical predictions.

The observed trends in signal intensities also supports our earlier interpretation of the data being due to the ionization of the dimer rather than ionization of a monomeric structure and dimerization after ionization.

Conclusions:

Soot inception in combustion environments remains an intriguing research topic and our understanding on the dominant species involved in this process is still not complete. Based on the thermodynamic stability of PAHs and the experimental evidence of aromatic excimers in flames, most combustion chemistry mechanisms include irreversible pyrene dimerization as the particle inception step. However, pyrene dimers have never been observed directly and theoretical work questions the dominant role of such dimers. To add to this discussion, we described here a newly developed experimental approach based on flame-sampling tandem mass spectrometry to detect and identify PAH dimers. However, the flame-sampled mass spectra at various dilution ratios indicated that the observed dimers were generated in the sampling line, thus implying that pyrene dimers do not exist in the elevated temperature environments of flames and therefore cannot be important species in the particle inception step under these conditions. A similar conclusion should then also be true for dimers of PAHs smaller than pyrene given the fact that the forces holding such dimers together would be even weaker. For future work it is suggested to look for PAH dimers at different conditions, *i.e.* lower temperatures, and for dimers of

larger PAHs. With the focus of this study on the high-temperature environments of flames, the presented findings explicitly do not rule out the existence of pyrene dimers in cold environments found on other planets and their moons.

Acknowledgments:

The experiments were conducted at the Combustion Research Facility, Sandia National Laboratories, Livermore, CA. Support for this work was provided by Sandia National Laboratories under the Laboratory-Directed Research and Development (LDRD) program. Sandia National Laboratories is a multi-mission laboratory managed and operated by National Technology and Engineering Solutions of Sandia, LLC., a wholly owned subsidiary of Honeywell International, Inc., for the U.S. Department of Energy's National Nuclear Security Administration under contract DE-NA0003525. M.A. is supported by the Director, Office of Science, Office of Basic Energy Sciences, of the US Department of Energy under contract no. DE-AC02-05CH11231, through the Gas Phase Chemical Physics Program, Chemical Sciences Division. The authors gratefully acknowledge Paul Fugazzi for technical assistance and Stephen Klippenstein (Argonne National Laboratory) for helpful discussions.

References:

1. Bockhorn, H., *Combustion Generated Fine Carbonaceous Particles*. KIT Scientific Publishing: 2009.
2. D'Anna, A. Combustion-Formed Nanoparticles. *Proc. Combust. Inst.* **2009,** *32*, 593-613.
3. Frenklach, M. Reaction Mechanism of Soot Formation in Flames. *Phys. Chem. Chem. Phys.* **2002,** *4*, 2028-2037.
4. Wang, H. Formation of Nascent Soot and Other Condensed-Phase Materials in Flames. *Proc. Combust. Inst.* **2011,** *33*, 41-67.
5. Hansen, N.; Miller, J. A.; Klippenstein, S. J.; Westmoreland, P. R.; Kohse-Höinghaus, K. Exploring Formation Pathways of Aromatic Compounds in Laboratory-Based Model Flames of Aliphatic Fuels. *Combust. Expl. Shock Waves* **2012,** *48*, 508-515.
6. McEnally, C. S.; Pfefferle, L. D.; Atakan, B.; Kohse-Höinghaus, K. Studies of Aromatic Hydrocarbon Formation Mechanisms in Flames: Progress Towards Closing the Fuel Gap. *Progr. Energy Combust. Sci.* **2006,** *32*, 247-294.
7. Miller, J. A.; Pilling, M. J.; Troe, J. Unravelling Combustion Mechanisms through a Quantitative Understanding of Elementary Reactions. *Proc. Combust. Inst.* **2005,** *30*, 43-88.
8. Richter, H.; Howard, J. B. Formation of Polycyclic Aromatic Hydrocarbons and Their Growth to Soot—a Review of Chemical Reaction Pathways. *Progr. Energy Combust. Sci.* **2000,** *26*, 565-608.
9. Johansson, K. O.; Dillstrom, T.; Elvati, P.; Campbell, M. F.; Schrader, P. E.; Popolan-Vaida, D. M.; Richards-Henderson, N. K.; Wilson, K. R.; Violi, A.; Michelsen, H. A. Radical–Radical Reactions, Pyrene Nucleation, and Incipient Soot Formation in Combustion. *Proc. Combust. Inst.* **2017,** *36*, 799-806.
10. Frenklach, M.; Wang, H. Detailed Modeling of Soot Particle Nucleation and Growth. *Proc. Combust. Inst.* **1991,** *23*, 1559-1566.
11. Golan, A.; Ahmed, M.; Mebel, A. M.; Kaiser, R. I. A VUV Photoionization Study of the Multichannel Reaction of Phenyl Radicals with 1,3-Butadiene under Combustion Relevant Conditions. *Phys. Chem. Chem. Phys.* **2013,** *15*, 341-347.
12. Parker, D. S.; Kaiser, R. I.; Bandyopadhyay, B.; Kostko, O.; Troy, T. P.; Ahmed, M. Unexpected Chemistry from the Reaction of Naphthyl and Acetylene at Combustion-Like Temperatures. *Angew. Chem. Int. Ed.* **2015,** *54*, 5421-5424.
13. Parker, D. S.; Kaiser, R. I.; Troy, T. P.; Ahmed, M. Hydrogen Abstraction/Acetylene Addition Revealed. *Angew. Chem. Int. Ed.* **2014,** *53*, 7740-7744.

14. Zhang, F.; Kaiser, R. I.; Kislov, V. V.; Mebel, A. M.; Golan, A.; Ahmed, M. A VUV Photoionization Study of the Formation of the Indene Molecule and Its Isomers. *J. Phys. Chem. Lett.* **2011,** *2*, 1731-1735.
15. Zhao, L.; Kaiser, R. I.; Xu, B.; Ablikim, U.; Ahmed, M.; Joshi, D.; Veber, G.; Fischer, F. R.; Mebel, A. M. Pyrene Synthesis in Circumstellar Envelopes and Its Role in the Formation of 2d Nanostructures. *Nature Astronomy* **2018,** *2*, 413-419.
16. León, L.; Ruwe, L.; Moshammer, K.; Seidel, L.; Shrestha, K. P.; Wang, X.; Mauss, F.; Kohse-Höinghaus, K.; Hansen, N. Chemical Insights into the Larger Sooting Tendency of 2-Methyl-2-Butene Compared to N-Pentane. *Combust. Flame* **2019,** *208*, 182-197.
17. Moshammer, K.; Seidel, L.; Wang, Y.; Selim, H.; Sarathy, S. M.; Mauss, F.; Hansen, N. Aromatic Ring Formation in Opposed-Flow Diffusive 1, 3-Butadiene Flames. *Proc. Combust. Inst.* **2017,** *36*, 947-955.
18. Ruwe, L.; Moshammer, K.; Hansen, N.; Kohse-Höinghaus, K. Consumption and Hydrocarbon Growth Processes in a 2-Methyl-2-Butene Flame. *Combust. Flame* **2017,** *175*, 34-46.
19. Ruwe, L.; Moshammer, K.; Hansen, N.; Kohse-Höinghaus, K. Influences of the Molecular Fuel Structure on Combustion Reactions Towards Soot Precursors in Selected Alkane and Alkene Flames. *Phys. Chem. Chem. Phys.* **2018,** *20*, 10780-10795.
20. Shukla, B.; Koshi, M. A Novel Route for PAH Growth in HACA Based Mechanisms. *Combust. Flame* **2012,** *159*, 3589-3596.
21. Shukla, B.; Miyoshi, A.; Koshi, M. Role of Methyl Radicals in the Growth of PAHs. *J. Am. Soc. Mass Spectrom.* **2010,** *21*, 534-544.
22. Shukla, B.; Susa, A.; Miyoshi, A.; Koshi, M. Role of Phenyl Radicals in the Growth of Polycyclic Aromatic Hydrocarbons. *J. Phys. Chem. A* **2008,** *112*, 2362-2369.
23. Hansen, N.; Schenk, M.; Moshammer, K.; Kohse-Höinghaus, K. Investigating Repetitive Reaction Pathways for the Formation of Polycyclic Aromatic Hydrocarbons in Combustion Processes. *Combust. Flame* **2017,** *180*, 250-261.
24. Schuetz, C. A.; Frenklach, M. Nucleation of Soot: Molecular Dynamics Simulations of Pyrene Dimerization. *Proc. Combust. Inst.* **2002,** *29*, 2307-2314.
25. Elvati, P.; Violi, A. Thermodynamics of Poly-Aromatic Hydrocarbon Clustering and the Effects of Substituted Aliphatic Chains. *Proc. Combust. Inst.* **2013,** *34*, 1837-1843.
26. Sabbah, H.; Biennier, L.; Klippenstein, S. J.; Sims, I. R.; Rowe, B. R. Exploring the Role of PAHs in the Formation of Soot: Pyrene Dimerization. *J. Phys. Chem. Lett.* **2010,** *1*, 2962-2967.

27. Totton, T. S.; Misquitta, A. J.; Kraft, M. A Quantitative Study of the Clustering of Polycyclic Aromatic Hydrocarbons at High Temperatures. *Phys. Chem. Chem. Phys.* **2012,** *14*, 4081-4094.
28. Kholghy, M. R.; Kelesidis, G. A.; Pratsinis, S. E. Reactive Polycyclic Aromatic Hydrocarbon Dimerization Drives Soot Nucleation. *Phys. Chem. Chem. Phys.* **2018,** *20*, 10926-10938.
29. Miller, J. H. Aromatic Excimers: Evidence for Polynuclear Aromatic Hydrocarbon Condensation in Flames. *Proc. Combust. Inst.* **2005,** *30*, 1381-1388.
30. Miller, J. H. The Kinetics of Polynuclear Aromatic Hydrocarbon Agglomeration in Flames. *Proc. Combust. Inst.* **1991,** *23*, 91-98.
31. Eaves, N. A.; Dworkin, S. B.; Thomson, M. J. The Importance of Reversibility in Modeling Soot Nucleation and Condensation Processes. *Proc. Combust. Inst.* **2015,** *35*, 1787-1794.
32. Eaves, N. A.; Dworkin, S. B.; Thomson, M. J. Assessing Relative Contributions of PAHs to Soot Mass by Reversible Heterogeneous Nucleation and Condensation. *Proc. Combust. Inst.* **2017,** *36*, 935-945.
33. Keller, M.; de Bruin, T.; Matrat, M.; Nicolle, A.; Catoire, L. A Theoretical Multiscale Approach to Study the Initial Steps Involved in the Chemical Reactivity of Soot Precursors. *Energy Fuels* **2019,** *33*, 10255-10266.
34. Giordana, A.; Maranzana, A.; Tonachini, G. Carbonaceous Nanoparticle Molecular Inception from Radical Addition and Van Der Waals Coagulation of Polycyclic Aromatic Hydrocarbon-Based Systems. A Theoretical Study. *J. Phys. Chem. C* **2011,** *115*, 17237-17251.
35. Adamson, B. D.; Skeen, S. A.; Ahmed, M.; Hansen, N. Detection of Aliphatically Bridged Multi-Core Polycyclic Aromatic Hydrocarbons in Sooting Flames with Atmospheric-Sampling High-Resolution Tandem Mass Spectrometry. *J. Phys. Chem. A* **2018,** *122*, 9338-9349.
36. Chung, S.-H.; Violi, A. Peri-Condensed Aromatics with Aliphatic Chains as Key Intermediates for the Nucleation of Aromatic Hydrocarbons. *Proc. Combust. Inst.* **2011,** *33*, 693-700.
37. Totton, T. S.; Misquitta, A. J.; Kraft, M. A Transferable Electrostatic Model for Intermolecular Interactions between Polycyclic Aromatic Hydrocarbons. *Chem. Phys. Lett.* **2011,** *510*, 154-160.
38. Wong, D.; Whitesides, R.; Schuertz, C.; Frenklach, M. Molecular Dynamics Simulations of PAH Dimerization. In *Combustion Generated Fine Carbonaceous Particles*, Bockhorn, H.; D'Anna, A.; Sarofim, A. F.; Wang, H., Eds. KIT Publishing, Karlsruhe, 2009; pp 247-257.
39. Zhang, H.-B.; You, X.; Wang, H.; Law, C. K. Dimerization of Polycyclic Aromatic Hydrocarbons in Soot Nucleation. *J. Phys. Chem. A* **2014,** *118*, 1287-1292.

40. Mao, Q.; van Duin, A. C.; Luo, K. Formation of Incipient Soot Particles from Polycyclic Aromatic Hydrocarbons: A Reaxff Molecular Dynamics Study. *Carbon* **2017,** *121*, 380-388.
41. Mouton, T.; Mercier, X.; Desgroux, P. Isomer Discrimination of PAHs Formed in Sooting Flames by Jet-Cooled Laser-Induced Fluorescence: Application to the Measurement of Pyrene and Fluoranthene. *Applied Physics B* **2016,** *122*, 123.
42. Mitra, T.; Zhang, T.; Sediako, A. D.; Thomson, M. J. Understanding the Formation and Growth of Polycyclic Aromatic Hydrocarbons (PAHs) and Young Soot from N-Dodecane in a Sooting Laminar Coflow Diffusion Flame. *Combustion and Flame* **2019,** *202*, 33-42.
43. Olten, N.; Senkan, S. Formation of Polycyclic Aromatic Hydrocarbons in an Atmospheric Pressure Ethylene Diffusion Flame. *Combustion and Flame* **1999,** *118*, 500-507.
44. Stein, S. E.; Fahr, A. High-Temperature Stabilities of Hydrocarbons. *J. Phys. Chem.* **1985,** *89*, 3714-3725.
45. Johansson, K.; Lai, J.; Skeen, S.; Popolan-Vaida, D.; Wilson, K.; Hansen, N.; Violi, A.; Michelsen, H. Soot Precursor Formation and Limitations of the Stabilomer Grid. *Proc. Combust. Inst.* **2015,** *35*, 1819-1826.
46. Schenk, M.; Hansen, N.; Vieker, H.; Beyer, A.; Gölzhäuser, A.; Kohse-Höinghaus, K. PAH Formation and Soot Morphology in Flames of C_4 Fuels. *Proc. Combust. Inst.* **2015,** *35*, 1761-1769.
47. Egolfopoulos, F. N.; Hansen, N.; Ju, Y.; Kohse-Höinghaus, K.; Law, C. K.; Qi, F. Advances and Challenges in Laminar Flame Experiments and Implications for Combustion Chemistry. *Progr. Energy Combust. Sci.* **2014,** *43*, 36-67.
48. Hansen, N.; Tranter, R.; Randazzo, J.; Lockhart, J.; Kastengren, A. Investigation of Sampling-Probe Distorted Temperature Fields with X-Ray Fluorescence Spectroscopy. *Proc. Combust. Inst.* **2019,** *37*, 1401-1408.
49. Hansen, N.; Tranter, R. S.; Moshammer, K.; Randazzo, J. B.; Lockhart, J. P.; Fugazzi, P. G.; Tao, T.; Kastengren, A. L.; Flame 2d-Imaging of Sampling-Probe Perturbations in Laminar Premixed Flames Using Kr X-Ray Fluorescence. *Combust. Flame* **2017,** *181*, 214-224.
50. Struckmeier, U.; Oßwald, P.; Kasper, T.; Böhling, L.; Heusing, M.; Köhler, M.; Brockhinke, A.; Kohse-Höinghaus, K. Sampling Probe Influences on Temperature and Species Concentrations in Molecular Beam Mass Spectroscopic Investigations of Flat Premixed Low-Pressure Flames. *Z. Phys. Chem.* **2009,** *223*, 503-537.
51. Maricq, M. M. Size and Charge of Soot Particles in Rich Premixed Ethylene Flames. *Combust. Flame* **2004,** *137*, 340-350.

52. Maricq, M. M.; Harris, S. J.; Szente, J. J. Soot Size Distributions in Rich Premixed Ethylene Flames. *Combust. Flame* **2003,** *132*, 328-342.
53. Zhao, B.; Yang, Z.; Wang, J.; Johnston, M. V.; Wang, H. Analysis of Soot Nanoparticles in a Laminar Premixed Ethylene Flame by Scanning Mobility Particle Sizer. *Aerosol Sci. Techn.* **2003,** *37*, 611-620.
54. Saggese, C.; Cuoci, A.; Frassoldati, A.; Ferrario, S.; Camacho, J.; Wang, H.; Faravelli, T. Probe Effects in Soot Sampling from a Burner-Stabilized Stagnation Flame. *Combust. Flame* **2016,** *167*, 184-197.